Analysis and Comparison of High Frequency Resonance in Small and Large Scale DFIG System

Song, Yipeng; Blaabjerg, Frede; Wang, Xiongfei

Published in:
Proceedings of 8th IEEE Energy Conversion Congress and Exposition (ECCE), 2016

DOI (link to publication from Publisher):
10.1109/ECCE.2016.7854863

Publication date:
2016

Document Version
Publisher's PDF, also known as Version of record

Analysis and Comparison of High Frequency Resonance in Small and Large Scale DFIG System

Yipeng Song, Frede Blaabjerg, Xiongfei Wang
Department of Energy Technology, Aalborg University
Aalborg 9220, Denmark
yis@et.aau.dk, fbl@et.aau.dk, xwa@et.aau.dk

***Abstract* — When connected to a parallel compensated weak grid network, both the small and large power scale Doubly Fed Induction Generator (DFIG) system may suffer high frequency resonance (HFR) due to the impedance interaction between the DFIG system and the parallel compensated weak network. Since the parameters of the small and large scale DFIG systems, including DFIG machine parameters and the LCL filter parameters, may vary between 10 to 100 times, the impedance modeling results of small and large scale DFIG system are quite different. Based on the built impedance modeling results, the HFR in small and large scale DFIG system are theoretically analyzed and compared in this paper with the discussion on the influence of PI controller proportional parameters and the digital control delay on the DFIG system impedance shaping. The experimental validation of small scale DFIG system and the simulation validation of large scale DFIG system are conducted to verify the correctness of the analysis.**

***Keywords* — *DFIG system*, *high frequency resonance*, *small and large power scale*, *proportional parameter*, *digital control delay*.**

I. Introduction

As the demand for renewable power generation has continued to increase during the past few decades, the wind power generation has been under vast scale commercial operation with rapid growth. The Doubly Fed Induction Generator (DFIG) system has been widely employed as a popular solution of wind power generation [1]-[2] since the power rating of the DFIG converters are much smaller than the full scale wind energy generation such as Permanent Magnetic Synchronous Generators and Squirrel Cage Induction Generators.

Nevertheless, since the DFIG machine's stator winding and grid side converter output filter are directly connected to the power network, the DFIG system may be sensitive and vulnerable to the power network variation, such as grid voltage unbalance [3]-[4], harmonic distortion [5]-[6] and grid fault [7]-[10]. As analyzed in [11]-[17], due to the impedance interaction between the DFIG system and the series compensated weak power grid, the Sub- Synchronous Resonance (SSR) occurs when the DFIG system is connected to the series compensated power network, and the frequency of SSR is always below the fundamental frequency. It is pointed out in [11]-[15] that the SSR is produced due to the inductive behavior of the DFIG system and the capacitive behavior of the series compensated weak network. Besides, it is reported in [11] that the possibility of DFIG SSR becomes higher as the rotor speed becomes lower and the compensation level of the series compensated weak network becomes larger. The PI current controller parameters are proved to have certain influence on the SSR phenomenon, that is, the larger proportional parameter is more likely to produce SSR in [11]. The SSR active damping strategies for DFIG system have been investigated. One solution is to modify the impedance shape of the series compensated weak network through the implementation of Thyristor-Controlled Series Capacitor (TCSC) [16], which can flexibly adjust the value of the series compensated capacitance, then the potential SSR can be avoided. Another solution is to modify the impedance shape of the DFIG system with the virtual impedance [15], the impedance of the DFIG system can be appropriately reshaped through the virtual impedance to effectively mitigate the SSR. Both these two solutions aim at impedance reshaping on either the series compensated weak network or the DFIG system with the purpose of avoiding the impedance interaction and mitigating the SSR as a result.

In addition to the SSR phenomenon, the DFIG system is also likely to suffer from High Frequency Resonance (HFR) due to the impedance interaction between the DFIG system and the parallel compensated weak network. Since the small scale and large scale DFIG system parameters, mainly the DFIG machine parameters and the LCL filter parameters may vary between 10 to 100 times and as a result the DFIG system impedance will vary significantly. Consequently, the HFR of small and large scale DFIG system will also be different due to different impedance shapes.

Moreover, as long as one specific DFIG system is chosen, its system parameters can be regarded as constant values. However, the parameters of the PI controllers for the rotor current control in Rotor Side Converter (RSC) and converter side current control in Grid Side Converter (GSC) can be flexibly adjusted. Clearly, the PI controller parameters will influence the DFIG system impedance modeling result, and a detailed analysis on how the PI controller parameters influence the small and large scale DFIG system impedance modeling will be studied in this paper. Note that in all the digital control system, the digital control delay [18]-[20] is inevitable for the current closed-loop control, thus both current controls in RSC and GSC are subject to this delay. In

the following discussion, the digital control delay will be taken into consideration, which makes the impedance modeling result more accurate.

This paper is organized as follows: the general DFIG system impedance modeling which fits both small and large scale DFIG system is first discussed as a platform for the following analysis, and the PI controller is explained from the perspective of equivalent impedance in Section II. The HFR between the small or large scale DFIG system and parallel compensated power network is analyzed and compared in Section III. The experimental and simulation validation of the small and large scale DFIG system HFR are conducted in Section IV and Section V respectively. Finally, conclusions are given in Section VI.

II. DFIG System Impedance Modeling

In order better to explain the small and large scale DFIG system HFR, its impedance modeling needs first to be discussed. Note that an LCL filter, rather than conventional L filter, is used in GSC due to better switching harmonic filtering performance.

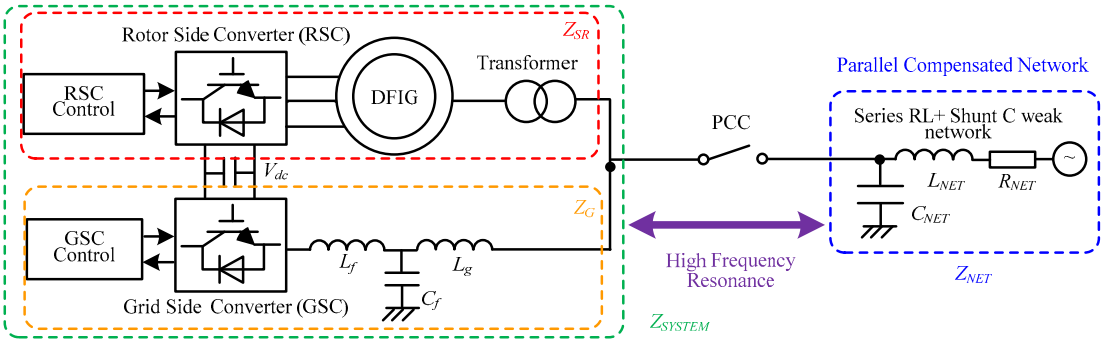

Fig. 1. Diagram of the DFIG system and a parallel compensated weak power network; RSC: Rotor Side Converter, GSC: Grid Side Converter.

TABLE I. Parameters of Small Scale 7.5 kW DFIG System

Rated Power	7.5 kW	Voltage Level	380 V
L_g	7 mH	L_f	11 mH
C_f	6.6 μF	L_m	79.3 mH
$L_{\sigma s}$	3.44 mH	$L_{\sigma r}$	5.16 mH
R_s	0.44 Ω	R_r	0.64 Ω
K_{prsc}	4	K_{irsc}	9
K_{pgsc}	4	K_{igsc}	9
f_s	10 kHz	f_{sw}	5 kHz

TABLE II. Parameters of Large Scale 2MW DFIG System

Rated Power	2 MW	Voltage Level	690 V
L_g	125 μH	L_f	125 μH
C_f	220 μF	L_m	3 mH
$L_{\sigma s}$	0.04 mH	$L_{\sigma r}$	0.06 mH
R_s	0.0015 Ω	R_r	0.0016 Ω
K_{prsc}	0.2	K_{irsc}	0.7
K_{pgsc}	0.3	K_{igsc}	0.5
f_s	5 kHz	f_{sw}	2.5 kHz

A. System Description

Fig. 1 shows the diagram of the DFIG system and parallel compensated weak power network. The parameters of the small and large scale DFIG system are available in Table I and Table II respectively. The RSC controls the rotor voltage to implement the DFIG machine stator output active and reactive power, the GSC is responsible for providing a stable dc-link voltage for the RSC, and an LCL filter is adopted due to better switching frequency harmonic filtering performance. For the purpose of preventing inrush current during grid connection and inner system current circulation, a transformer is connected between the DFIG stator winding and Point of Common Coupling (PCC). Since the transformer does not change the voltage level of the primary side and the secondary side, it will be neglected during the impedance modeling in the following sections.

For the parallel compensated weak network, it consists of the network resistance R_{NET} and network inductance L_{NET} in series connection and these two parameters exist due to the long-distance transmission line. The parallel compensated capacitance C_{NET} occurs due to the parasitic capacitance between transmission line and ground, and also may derive from a power factor correction capacitance. Thus it can be seen that the parallel compensated weak network is likely to occur in the practical application scenario.

B. DFIG system impedance modeling

This section discusses the DFIG system impedance modeling, which includes the grid part and the machine part.

For the DFIG system grid part including the GSC and output LCL filter, which can be similarly regarded as the grid-connected converter, the impedance modeling of the LCL filter based grid-connected converter has been well investigated in [18]-[20] and can be directly used here as shown in Fig. 2.

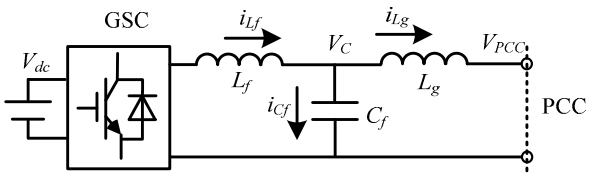

(a)

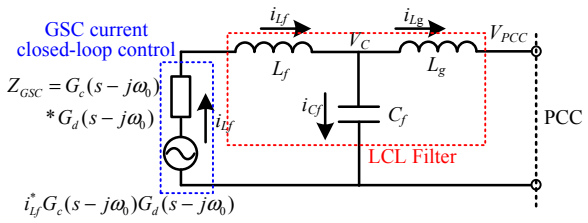

(b)

Fig. 2. GSC with LCL filter (a) equivalent circuit and (b) impedance modeling

It can be seen from Fig. 2(a) that the GSC control has an outer control loop of the dc-link voltage. However, the control bandwidth of dc-link voltage is typically less than 100 Hz and this means the dc-link capacitance has much longer time constant and thus the outer control loop of dc-link voltage is neglected [11] when investigating the HFR. Similarly, the grid synchronization with Phase Locked Loop (PLL) can also be neglected due to the similar slow dynamic characteristics as the dc-link voltage control [11].

Based on Fig. 2, the impedance Z_G of GSC and LCL filter seen from the PCC can be presented as [18]-[20],

$$Z_G = \frac{Z_{Cf}\left(Z_{Lf}+Z_{GSC}\right)+Z_{Lg}\left(Z_{Lf}+Z_{GSC}\right)+Z_{Cf}Z_{Lg}}{Z_{Cf}+\left(Z_{Lf}+Z_{GSC}\right)} \quad (1)$$

where, the GSC current control is modeled as one voltage source $i_{Lf}^* G_c(s\text{-}j\omega_0)G_d(s\text{-}j\omega_0)$ and one impedance $Z_{GSC} = G_c(s\text{-}j\omega_0)G_d(s\text{-}j\omega_0)$ in series. $G_c(s\text{-}j\omega_0)$ is the PI controller containing the proportional part K_{pgsc} and the integral part $K_{igsc}/(s\text{-}j\omega_0)$, which can be found in Table I and Table II. $G_d(s\text{-}j\omega_0)$ is the digital control delay of 1.5 sampling period, which can be expressed as $G_d(s) = e^{-sTd}$. $Z_{Cf} = 1/sC_f$, $Z_{Lf} = sL_f$, $Z_{Lg} = sL_g$, C_f is the LCL filter capacitor, L_f is the LCL filter inductor connected to the converter, L_g is the LCL filter inductor connected to the grid network. $\omega_0 = 100\pi$ rad/s is the grid fundamental component angular speed, and it is introduced to denote the rotation from the stationary frame to the synchronous frame where the PI closed-loop current regulation is implemented.

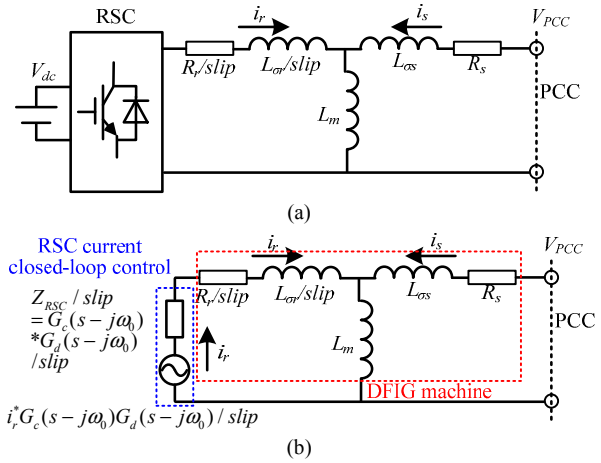

(b)

Fig. 3. RSC and DFIG machine (a) equivalent circuit and (b) impedance modeling

The impedance modeling of RSC and DFIG machine has been reported in [11] to analyze the DFIG system SSR phenomenon. Obviously, this impedance modeling result can be adopted to analyze the HFR as well. As a platform for the following analysis, the circuit and impedance modeling of RSC and DFIG machine [11] need to be mentioned here as shown in Fig. 3.

Since the rotor current control and output voltage are both represented in the rotor reference frame, they need to be rotated to the stationary frame by the slip angular speed expressed as [11]-[15],

$$slip = \left(s - j\omega_r\right)/s \quad (2)$$

where ω_r is the rotor angular speed.

Then, according to Fig. 3, the impedance Z_{SR} of RSC and DFIG machine seen from the PCC can be obtained as [11],

$$Z_{SR} = \frac{Z_{Lm}H/slip+\left(R_s+Z_{L\sigma s}\right)H/slip+Z_{Lm}\left(R_s+Z_{L\sigma s}\right)}{Z_{Lm}+H/slip} \quad (3)$$

where, $H = R_r + Z_{L\sigma r} + Z_{RSC}$; $Z_{RSC} = G_c(s\text{-}j\omega_0)G_d(s\text{-}j\omega_0)$; $Z_{Lm} = sL_m$; $Z_{L\sigma r} = sL_{\sigma r}$; $Z_{L\sigma s} = sL_{\sigma s}$.

As it is shown in Fig. 1, the RSC and DFIG machine, together with the GSC and LCL filter, are connected in parallel to the PCC. While the dc-link capacitor has the function of decoupling the control of the RSC and GSC due to the well-regulated constant dc-link voltage, then the DFIG system impedance can be derived based on the parallel connection of the grid part in (1) and machine part in (3),

$$Z_{SYSTEM} = Z_G Z_{SR}/\left(Z_G + Z_{SR}\right) \quad (4)$$

C. Analysis of PI controller parameters with the consideration of digital control delay

As it can be observed from Fig. 2(b) and Fig. 3(b), the only adjustable parameters in the DFIG system impedance modeling are the PI controller parameters in the RSC and GSC. Therefore, the influence of PI controller parameters on the DFIG system impedance needs to be discussed and the inevitable digital control delay should also be taken into consideration.

The PI controller consists of proportional part and integral part as,

$$G_c(s) = K_p + K_i/s \quad (5)$$

where, K_p and K_i are the proportional and integral parameters.

Since the HFR is always at high frequency range (> 800 Hz), the integral part can be neglected at this high frequency, thus only the proportional part K_p will influence the DFIG system impedance in the high frequency range.

From the perspective of equivalent impedance, the proportional part can be regarded as a virtual resistance as shown in Fig. 4(a). Importantly the digital control delay is inevitable and must be taken into consideration, thus the proportional part is transformed to the combination of a

virtual positive resistance and positive capacitance (or negative inductance) as shown in Fig. 4(b) and Fig. 4(c). According to Table I and Table II, the sampling frequencies for small and large scale DFIG system are 10 kHz and 5 kHz respectively, thus the digital control delay of 1.5 times sampling period is 150 μs and 300 μs respectively.

Clearly, different impedance shaping results can be obtained for different control delays in small and large scale DFIG system: 1) for the small scale DFIG system shown in Fig. 4(b), within the interested HFR frequency range (around 800 Hz to1600 Hz), the proportional parameter can be transformed to the combination of Positive Resistance (PR) and Negative Inductance (NL). 2) On the other hand, for the large scale DFIG system as shown in Fig. 4(c), due to the comparatively larger digital control delay, the proportional parameter can be transformed to the combination of Negative Resistance (NR) and Negative Inductance (NL).

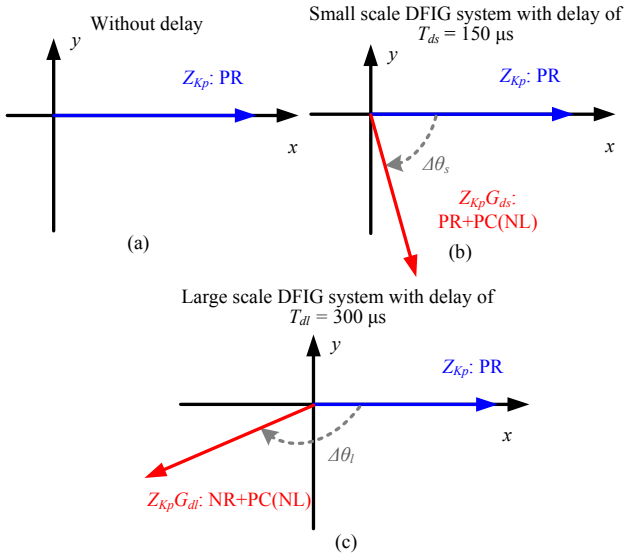

Fig. 4. Equivalent impedance of proportional part of PI controller in the high frequency range (a) without digital control delay; (b) small scale DFIG with digital control delay of T_{ds} = 150 μs; (c) large scale DFIG with digital control delay of T_{dl} =300 μs. PR: Positive Resistance, NR: Negative Resistance, PC: Positive Capacitance, NL: Negative Inductance.

Obviously, based on Fig. 4, it can be found that large K_p results in large negative inductance. As a consequence, the rotor branch in RSC and the converter branch in GSC of the large scale DFIG system may change from their original inductive character to capacitive character due to the large negative inductance and small DFIG system parameters. Thus, it is essential to determine the appropriate proportional parameter K_p in order to maintain the inductive character of the large scale DFIG system. On the other hand, for the small scale DFIG system, the DFIG system parameters are much larger than the proportional parameter K_p, thus the variation of K_p has negligible influence on the small scale DFIG system impedance modeling.

For the Z_{SR} of the large scale DFIG system as shown in Fig. 3(b), the rotor branch impedance can be presented as, (K_{irsc} and R_r are neglected due to small values at the high frequency range)

$$\begin{aligned}&\left(K_{prsc}+K_{irsc}/s\right)e^{-sT_d}/slip+\left(R_r+sL_{\sigma r}\right)/slip\approx\\&\left(K_{prsc}\cos(\omega T_d)-jK_{prsc}\sin(\omega T_d)+j\omega L_{\sigma r}\right)/slip\end{aligned}\tag{6}$$

In order to ensure the inductive character of the rotor branch in RSC, the imagine part of (6) should be larger than 0, the following equation considering K_{prsc} must be fulfilled,

$$K_{prsc}<\omega L_{\sigma r}/\sin(\omega T_d)\tag{7}$$

where, $L_{\sigma r}$ is the rotor leakage inductance.

Similarly, for the Z_G of large scale DFIG system shown in Fig. 2(b), the converter filter branch impedance can be expressed as, (K_{igsc} is neglected due to small values at the high frequency range)

$$\begin{aligned}&\left(K_{pgsc}+K_{igsc}/s\right)e^{-sT_d}+sL_f\approx\\&K_{pgsc}\cos(\omega T_d)-jK_{pgsc}\sin(\omega T_d)+j\omega L_f\end{aligned}\tag{8}$$

In order to ensure the inductive character of converter filter branch in the GSC, the imagine part of (8) should be larger than 0, the following equation regarding K_{pgsc} must be met,

$$K_{pgsc}<\omega L_f/\sin(\omega T_d)\tag{9}$$

Note that, for the case of large scale DFIG system shown in Fig. 4(c), the largest magnitude of negative inductance occurs at 833 Hz with the delay angle $\Delta\theta_l$ = 90°. Thus, the proportional parameters for RSC and GSC should meet the requirements according to (7) and (9) respectively as K_{prsc} < 0.31, K_{pgsc} < 0.65.

Fig. 5 shows the Bode diagram of small and large scale DFIG system impedance. As it can be seen from Fig. 5(a), due to the large value of the small scale DFIG system parameters as shown in Table I, the K_p, i.e., K_{prsc} = 4, K_{irsc} = 9, K_{pgsc} = 4, K_{igsc} = 9, has negligible influence on the DFIG system impedance shape, and the impedance Z_{SR} is able to maintain inductive in the high frequency range. The only capacitive character exists in the Z_G due to the LCL filter. Thus, the system impedance Z_{SYSTEM} behaves capacitive around 800 Hz - 1000 Hz, while it behaves inductive at the rest of the frequency ranges.

For the large scale DFIG system with appropriate parameters K_{prsc} = 0.3, K_{irsc} = 2, K_{pgsc} = 0.6, K_{igsc} = 2 as shown in Fig. 5(b), both Z_{SR} and Z_G behave as a combination of negative resistance (caused by the K_p and control delay T_d) and positive inductance (due to the inherent inductive character of Z_{SR} and Z_G), thus the phase response is kept between 90° and 180°.

In contrast, when inappropriately large proportional parameters K_{prsc} = 0.6, K_{irsc} = 2, K_{pgsc} = 1.2, K_{igsc} = 2 are used as shown in Fig. 5(c), the impedance of Z_{SR} is different, i.e., it behaves as a combination of negative resistance and negative inductance with a phase response between -90° and -180° from 833 Hz to 925 Hz, and then behaves as the combination of negative resistance and positive inductance with a phase response between -180° and -270° above 925

Hz. On the other hand, Z_G remains the same as in Fig. 5(b). As a result, the overall system impedance Z_{SYSTEM} has similar shaping of Z_{SR} which is quite different from that shown in Fig. 5(b).

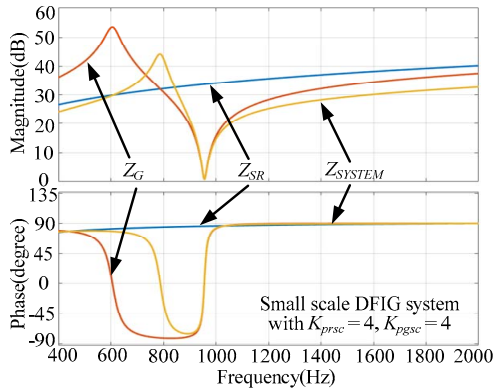

(a)

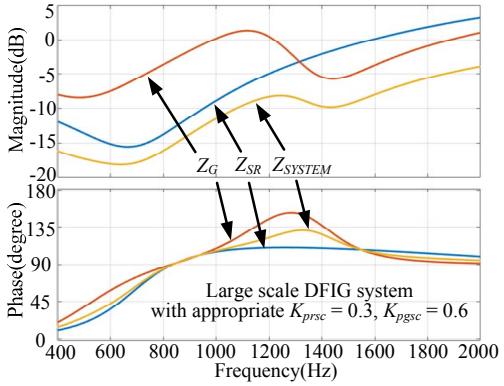

(b)

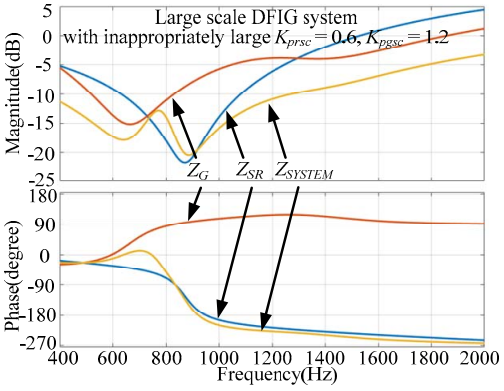

(c)

Fig. 5. Bode diagram of DFIG system impedance (a) small scale DFIG system with K_{prsc} = 4, K_{irsc} = 9, K_{pgsc} = 4, K_{igsc} = 9; (b) large scale DFIG system with appropriate K_{prsc} = 0.3, K_{irsc} = 2, K_{pgsc} = 0.6, K_{igsc} = 2; (c) large scale DFIG system with inappropriately large Kprsc = 0.6, K_{irsc} = 2, K_{pgsc} = 1.2, K_{igsc} = 2

Therefore, it can be concluded that the variations of PI controller proportional parameters have negligible influence on the small scale DFIG system due to the large value of DFIG system parameters, while they influence significantly the impedance shaping of the large scale DFIG system due to the small value of the DFIG system parameters. As a result, the appropriate PI controller proportional parameters need to be carefully selected to ensure the appropriate inductive DFIG system impedance shaping.

III. HFR OF SMALL AND LARGE SCALE DFIG SYSTEM

This section discusses the HFR between small and large scale DFIG system and the parallel compensated network (series RL + shunt C).

According to Fig. 1, the parallel compensated network impedance can be presented as,

$$Z_{NET} = \frac{\left(sL_{NET} + R_{NET}\right)/sC_{NET}}{sL_{NET} + R_{NET} + 1/sC_{NET}} \tag{10}$$

where, R_{NET} and L_{NET} are the network resistance and inductance in series, and C_{NET} is the network shunt capacitance.

Fig. 6 shows the Bode diagrams of (a) small scale / (b) large scale DFIG system impedance and the parallel compensated network impedance. The weak power network in Fig. 6(a) consists of series R_{NETS} = 3 mΩ, L_{NETS} = 1 mH, shunt C_{NETS} = 20 μF and the parameters of small scale DFIG system are given in Table I; while the network in Fig. 6(b) consists of series R_{NETL}= 3 mΩ, L_{NETL}= 0.1 mH, shunt C_{NETL} = 300 μF, the parameters of large scale DFIG system are given in Table II. The subscript 'S' and 'L' denote the case of small and large scale DFIG system respectively.

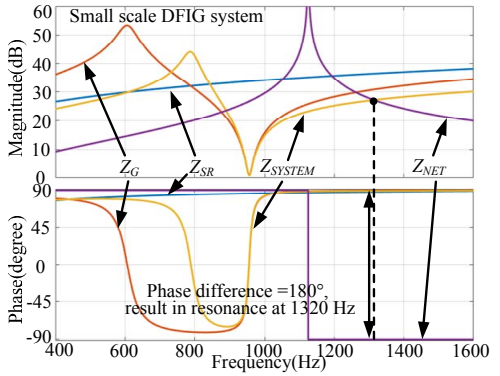

(a)

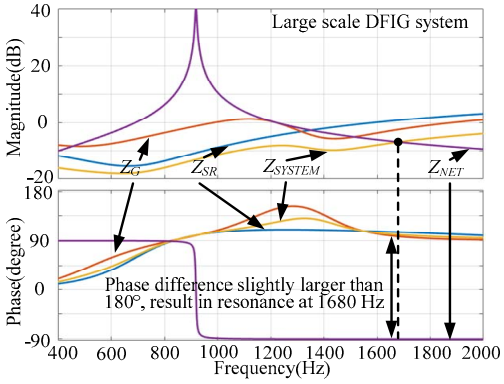

(b)

Fig. 6. Bode diagram of (a) small scale and (b) large scale DFIG system impedance and the parallel compensated network impedance

According to Fig. 6(a), the small scale DFIG system has one magnitude intersection point with the parallel compensated network, and the phase difference at this point is 180°, causing a HFR of 1320 Hz. Although there is one magnitude intersection point at 900 Hz, but the phase difference is around 160°, thus no resonance at this frequency will occur.

Similarly, for the large scale DFIG system in Fig. 6(b), the magnitude intersection point exists at 1680 Hz with a phase difference slightly larger than 180°, thus causing a HFR in the large scale DFIG system as well. Note that the phase response of DFIG system slightly larger than 90° indicates that the DFIG system equivalent resistance is negative, thus further aggravating the resonance to instability operation, which can be proved in the simulation validation section.

Therefore, it can be found that both small scale and large scale DFIG system may suffer from HFR when connected to the parallel compensated weak network, while the different resonance frequencies are determined mainly by the DFIG system parameters, proportional parameters of PI controller, digital control delay, as well as the weak network parameters.

IV. Experimental Validation for Small Power Scale DFIG System

In order to experimentally validate the DFIG system impedance modeling result and the HFR, a down-scaled 7.5 kW test rig is built up and shown in Fig. 7, with its parameters available in Table I. The DFIG is externally driven by a prime motor, and two 5.5-kW Danfoss motor drives are used for the GSC and the RSC, both of which are controlled with dSPACE 1006 control system. The rotor speed is set 1200 rpm (0.8 pu), the dc-link voltage is 650 V. The DFIG stator output active and reactive power are set to 5 kW and 0 Var respectively. The sampling and switching frequency of both converters are 10 kHz and 5 kHz respectively.

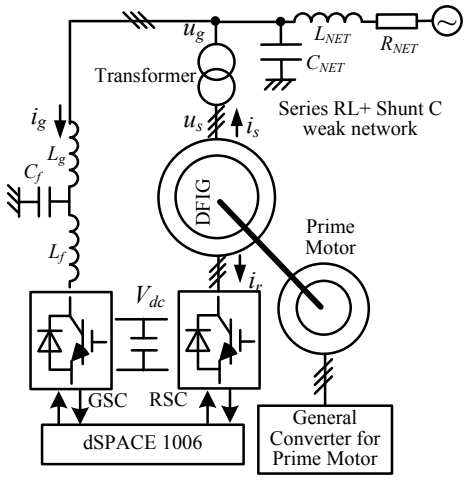

Fig. 7. Setup of a 7.5 kW DFIG system test rig

It should be pointed out that the experiment validation is conducted under weak network parameters of R_{NET} = 3 mΩ, L_{NET} = 1.5 mH, C_{NET} =15 μF, 10 μF, 5 μF. The Bode diagrams of these weak grid impedance and small scale DFIG system have been plotted in Fig. 8. As it can be seen, the theoretical analysis shows that the HFR of 1316 Hz, 1575 Hz and 2195 Hz will occur when the shunt capacitance C_{NET} is chosen as 15 μF, 10 μF and 5 μF respectively. The data are given out in Table III.

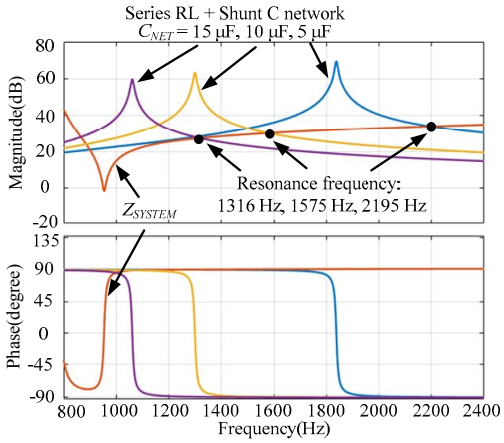

Fig. 8. Bode diagram of small scale DFIG system impedance and series RL + shunt C network impedance with C_{NET} =15, 10, 5 μF, R_{NET} = 3 mΩ, L_{NET} = 1.5 mH

TABLE III. Small Scale DFIG System HFR Theoretical Analysis and Experimental Results

Network Shunt Capacitor	Theoretical Analysis	Experimental Results
15 μF	1316 Hz	1475 Hz
10 μF	1575 Hz	1600 Hz
5 μF	2195 Hz	2250 Hz

Fig. 9 shows the experimental results of small scale DFIG system when the rotor speed is 1200 rpm (0.8 p.u. below the synchronous speed), weak grid network R_{NET} = 3 mΩ, L_{NET} = 1.5 mH, (a) C_{NET} = 15 μF; (b) C_{NET} = 10 μF; (c) C_{NET} = 5 μF. Obviously, due to the impedance interaction between the small scale DFIG system and the parallel compensated network, the HFR occurs, the stator voltage u_s, stator current i_s, rotor current i_r, grid voltage u_g and grid side current i_g all contain high frequency HFR components. The resonance frequency in the experimental results can be found to be 1475 Hz, 1600 Hz, and 2250 Hz respectively, which are shown in Table III.

By comparing the theoretical analysis and experimental results shown in Table III, it can be observed that the resonance frequency in the experimental results match well with the theoretical analysis within an acceptable error. This error can be attributed to the DFIG system parameters deviation due to temperature changing, skin effect and flux saturation, and also because of the weak network parameters deviation. Thus the correctness of the HFR theoretical analysis in the small scale DFIG system can be verified.

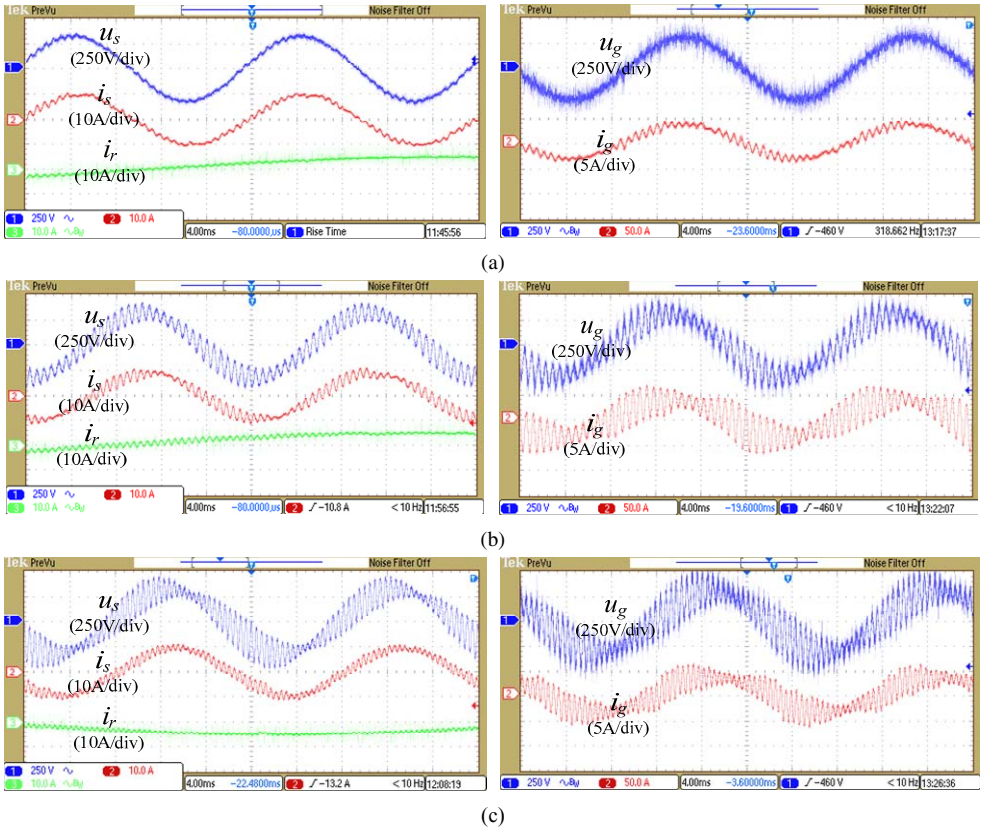

Fig. 9. Experimental result of 7.5 kW small scale DFIG system when rotor speed is 1200 rpm, weak grid network R_{NET} = 3 mΩ, L_{NET} = 1.5 mH, (a) C_{NET} = 15 μF; (b) C_{NET} = 10 μF; (c) C_{NET} = 5 μF. DFIG stator voltage u_s, stator current i_s and rotor current i_r, grid voltage u_g and grid side current i_g as shown.

V. Simulation Validation for Large Power Scale DFIG System

In order to validate the HFR of the large scale DFIG system, the simulation validation is provided based on MATLAB Simulink. The simulation of a 2 MW large scale DFIG system resonance is conducted with the weak network parameters of R_{NET} = 3 mΩ, L_{NET} = 0.1 mH, C_{NET} = 400 μF, 300 μF, 200 μF. The sampling and switching frequency of both converters are 5 kHz and 2.5 kHz respectively.

The Bode diagrams of these weak grid impedances and large scale DFIG system have been plotted in Fig. 10. The theoretical analysis shows that the large scale DFIG system HFR of 1530 Hz, 1680 Hz and 1960 Hz will occur when the shunt capacitance C_{NET} is chosen as 400 μF, 300 μF and 200 μF respectively, this data are available in Table IV.

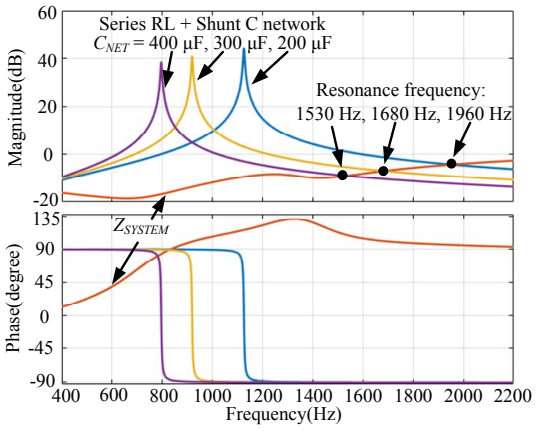

Fig. 10. Bode diagram of large scale DFIG system impedance and series RL + shunt C network impedance with R_{NET} = 3 mΩ, L_{NET} = 0.1 mH, C_{NET} = 400 μF, 300 μF, 200 μF.

TABLE IV. Large Scale DFIG System HFR Theoretical Analysis and Simulation Results

Network Shunt Capacitor	Theoretical Analysis	Simulation Results
400 μF	1530 Hz	1610 Hz
300 μF	1680 Hz	1720 Hz
200 μF	1960 Hz	2000 Hz

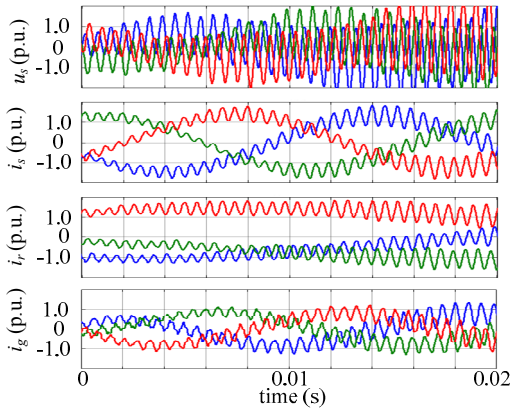

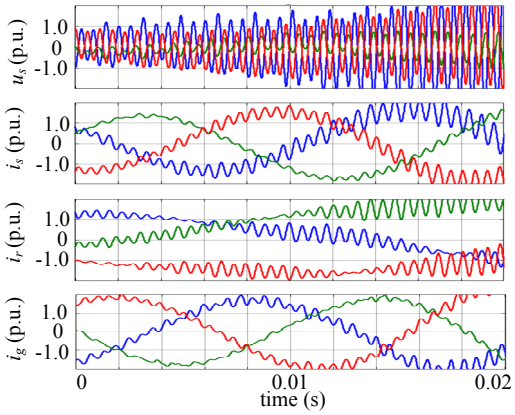

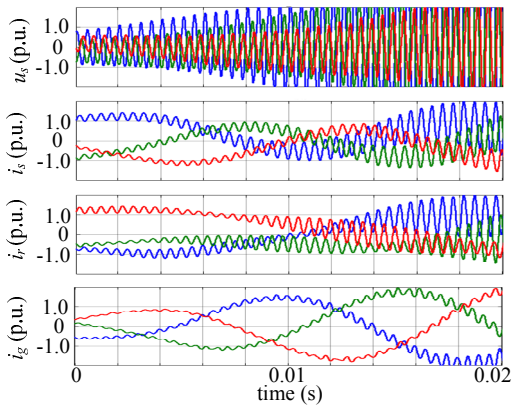

(c)

Fig. 11. Simulation results of 2 MW large scale DFIG system when rotor speed is 1200 rpm, weak grid network R_{NET} = 3 mΩ, L_{NET} = 0.1 mH, (a) C_{NET} = 400 μF; (b) C_{NET} = 300 μF; (c) C_{NET} = 200 μF. DFIG stator voltage u_s, stator current i_s and rotor current i_r, and grid side current i_g.

As it can be seen from Fig. 11, when the 2 MW DFIG system is connected to the parallel compensated network, the HFR of 1610 Hz, 1720 Hz and 2000 Hz occurs respectively with the shunt capacitance of 400 μF, 300 μF and 200 μF. The stator voltage, stator/rotor current and grid side current all contains the HFR components.

Most importantly, it can be observed that the DFIG system fails to operate stably due to the HFR. This can be explained as, the negative resistance shown in Fig. 6(b) helps to decrease the DFIG system equivalent resistance even to a negative value at the resonance frequency, thus resulting in the instability operation of the large scale DFIG system. Moreover, as shown in Table IV, the simulation results of HFR frequency matches well with the theoretical analysis with an acceptable frequency error. Thus, the HFR analysis of large scale DFIG system can be verified.

VI. Conclusion

This paper first established the DFIG system impedance modeling, including the RSC and DFIG machine, as well as the GSC and LCL filter. Then based on the established impedance modeling, the HFR of both small scale and large scale DFIG system when connected to the parallel compensated weak network is investigated. It is proved that both small and large scale DFIG may suffer HFR due to the phase difference of 180° at the magnitude intersection point. The PI controller proportional parameter K_p in the RSC and GSC has significant influence on the large scale DFIG system impedance shaping, thus also affecting the HFR behavior of the large scale DFIG system; while the K_p has negligible influence on the small scale DFIG system due to its comparatively large system parameters. The inevitable digital control delay needs to be considered to make the impedance modeling results of DFIG system more accurate.

REFERENCES

[1] F. Blaabjerg, and K. Ma, "Future on Power Electronics for Wind Turbine Systems," *IEEE J. Emer. Sel. Topics Power Electron*., vol. 1, no. 3, pp. 139-152, Sep. 2013.

[2] K. Ma, L. Tutelea, I. Boldea, D. M. Ionel, F. Blaabjerg, "Power Electronic Drives, Controls, and Electric Generators for Large Wind Turbines–An Overview", *Electric Power Components and Systems*, vol. 43, no. 12, pp. 1406-1421, 2015.

[3] H. Nian, P. Cheng, and Z. Q. Zhu, "Independent Operation of DFIG-Based WECS Using Resonant Feedback Compensators Under Unbalanced Grid Voltage Conditions," *IEEE Trans. Power Electron.*, vol. 30, no. 7, pp. 3650 - 3661, July 2015.

[4] H. Nian, P. Cheng, and Z. Q. Zhu, "Coordinated Direct Power Control of DFIG System Without Phase-Locked Loop Under Unbalanced Grid Voltage Conditions," *IEEE Trans. Power Electron.*, vol. 31, no. 4, pp. 2905 - 2918, April 2016.

[5] Y. Song, H. Nian, "Modularized Control Strategy and Performance Analysis of DFIG System Under Unbalanced and Harmonic Grid Voltage," *IEEE Trans. Power Electron.*, vol. 30, no. 9, pp. 4831 - 4842, Sept. 2015.

[6] H. Nian, Y. Song, "Direct Power Control of Doubly Fed Induction Generator Under Distorted Grid Voltage," *IEEE Trans. Power Electron.*, vol. 29, no. 2, pp. 894-905, Feb. 2014.

[7] R. Zhu, Z. Chen, Y. Tang, F. Deng, and X Wu, "Dual-Loop Control Strategy for DFIG-Based Wind Turbines Under Grid Voltage Disturbances," *IEEE Trans. Power Electron*., vol. 31, no. 3, pp. 2239 - 2253, Mar. 2016.

[8] W. Chen, F. Blaabjerg, N. Zhu, M. Chen, and D. Xu, "Doubly Fed Induction Generator Wind Turbine Systems Subject to Recurring Symmetrical Grid Faults," *IEEE Trans. Power Electron*., vol. 31, no. 2, pp. 1143 - 1160, Feb. 2016.

[9] D. Zhou, F. Blaabjerg, T. Franke, M. Lau, and M. Tonnes, "Reduced Cost of Reactive Power in Doubly Fed Induction Generator Wind Turbine System With Optimized Grid Filter", *IEEE Trans. Power Electron.*, vol. 30, no. 10, pp. 5581-5590, Oct. 2015.

[10] D. Zhou, F. Blaabjerg, T. Franke, M. Tonnes, and M. Lau, "Optimized Reactive Power Flow of DFIG Power Converters for Better Reliability Performance Considering Grid Codes.", *IEEE Trans. Ind. Electron.*, vol. 62, no. 3, pp. 1552-1562, Mar. 2015.

[11] Z. Miao, "Impedance-Model-Based SSR Analysis for Type 3 Wind Generator and Series-Compensated Network," *IEEE Trans. Energy Convers.*, vol. 27, no. 4, pp. 984–991, Dec. 2012.

[12] L. Fan, and Z. Miao, "Nyquist-Stability-Criterion-Based SSR Explanation for Type-3 Wind Generators," *IEEE Trans. Energy Convers.*, vol. 27, no. 3, pp. 807–809, Sep. 2012.

[13] I. Vieto, and J. Sun, "Small-Signal Impedance Modelling of Type-III Wind Turbine," *in Proc. Power & Energy Society General Meeting (PESG)*, pp. 1-5, 2015.

[14] I. Vieto, and J. Sun, "Real-time simulation of subsynchronous resonance in Type-III wind turbines," *in Proc. Control and Modeling for Power Electronics (COMPEL)*, pp. 1-8, 2014

[15] I. Vieto, and J. Sun, "Damping of Subsynchronous Resonance Involving Type-III Wind Turbines," *in Proc. Control and Modeling for Power Electronics (COMPEL)*, pp. 1-8, 2015.

[16] L. Piyasinghe, Z. Miao, J. Khazaei, and L. Fan, "Impedance Model-Based SSR Analysis for TCSC Compensated Type-3 Wind Energy Delivery Systems," *IEEE Trans. Sustainable Energy.*, vol. 6, no. 1, pp. 179–187, Jan. 2015.

[17] L. Fan, and Z. Miao, "Mitigating SSR Using DFIG-Based Wind Generation," *IEEE Trans. Sustainable Energy.*, vol. 3, no. 3, pp. 349–358, July 2012.

[18] X. Wang, F. Blaabjerg, and Z. Chen, "Synthesis of Variable Harmonic Impedance in Inverter-Interfaced Distributed Generation Unit for Harmonic Damping Throughout a Distribution Network," *IEEE Trans. Ind. Appl*., vol. 48, no. 4, pp. 1407-1417, July-Aug. 2012.

[19] X. Wang, F. Blaabjerg, and P. C. Loh, "Grid-Current-Feedback Active Damping for LCL Resonance in Grid-Connected Voltage Source Converters," *IEEE Trans. Power Electron*., vol. 31, no. 1, pp. 213-223, Jan. 2016.

[20] X. Wang, F. Blaabjerg, and P. C. Loh, "Virtual RC Damping of LCL-Filtered Voltage Source Converters With Extended Selective Harmonic Compensation," *IEEE Trans. Power Electron*., vol. 30, no. 9, pp. 4726-4737, Sep. 2015.